

# Bases and dimensions of bivariate hierarchical tensor–product splines

Carlotta Giannelli\*, Bert Jüttler†

*Institute of Applied Geometry, Johannes Kepler University, Altenberger Str. 69, 4040 Linz, Austria*

## Abstract

We prove that the dimension of bivariate tensor–product spline spaces of bi–degree  $(d, d)$  with maximum order of smoothness on a multi–cell domain (more precisely, on a set of cells from a tensor–product grid) is equal to the number of tensor–product B–spline basis functions, defined by only single knots in both directions, acting on the considered domain. A certain reasonable assumption on the configuration of the cells is required.

This result is then generalized to the case of piecewise polynomial spaces, with the same smoothness properties mentioned above, defined on a multi–grid multi–cell domain (more precisely, on a set of cells from a hierarchy of tensor–product grids). Again, a certain reasonable assumption regarding the configuration of cells is needed.

Finally, it is observed that this construction corresponds to the classical definition of hierarchical B–spline bases. This allows to conclude that this basis spans the full space of spline functions on multi–grid multi–cell domains under reasonable assumptions.

*Keywords:* hierarchical B–splines, tensor–product basis, dimension, local refinement.

## 1 Introduction

### 1.1 Motivation and related works

Adaptive refinement of spline basis functions allows to localize changes in the control net so that the modification of a single control point will affect a limited region of the underlying geometric representation. Mesh refinement strategies constitute a fundamental component for the development of an effective approximation algorithm commonly used by standard surface reconstruction techniques. In the context of the numerical solution of partial differential equations, particular attention is currently devoted to this issue in connection with the emerging field of isogeometric analysis [3].

For this reason, refinement techniques which were originally introduced for standard geometric design applications, became the topic of recent studies, taking into account

---

\*carlotta.giannelli@jku.at

†bert.juettler@jku.at

the dual requirements of geometry and analysis. The resulting novel perspective motivated new research for the identification of geometric representations suitable for analysis which simultaneously satisfy the demand imposed by their use in the simulation framework and the accuracy of the geometrical model.

The extension of the isogeometric paradigm, originally introduced considering the NURBS model [11], with spline representations which allow local control of the refinement procedure has mainly focused on suitable applications [1, 6, 20] of the T-splines construction [22, 23]. Subsequently, alternative solutions based on the so-called polynomial splines over T-meshes [4, 5, 14] and on hierarchical B-splines [7, 12] have also been considered [18, 24].

In this setting, the analytical point of view, which joins the geometric perspective, outlined the desire of characterizing the space spanned by the set of basis functions used to approximate the solution. This motivated investigations on the linear independence of T-splines blending functions [2, 16], discussion about the dimension of related spline spaces [17] and the corresponding nested nature of these T-spline spaces [15].

The hierarchical approach seems to be a valid solution to circumvent the weak points of T-splines identified by these studies (locality of the refinement [6], linear dependence associated with particular T-meshes [2], complexity of the enhanced refinement algorithm needed to ensure the linear independence of the blending functions [21]), and also the reduced regularity which is required for most results concerning splines over T-meshes. This includes the dimension results for spline spaces over T-meshes in the case that the degree is at least  $2s + 1$  for splines with order of smoothness given by  $s$  that were derived in [4].

The hierarchical model allows complete control of the refinement by using a spline hierarchy whose levels identifies subsequent levels of refinement. We consider an *increasingly nested* sequence of tensor-product spline spaces  $V^0 \subset V^1 \subset \dots \subset V^{N-1}$ , together with a *decreasingly nested* sequence of domains  $\Omega^0 \supseteq \Omega^1 \supseteq \dots \supseteq \Omega^{N-1}$ . The cells of  $V^\ell$  in  $\Omega^\ell \setminus \Omega^{\ell+1}$  will be said to form a *multi-cell domain*. The union of these multi-cell domains will then be called a *multi-grid multi-cell domain*.

The simple idea of the hierarchical spline model is based on a suitable correlation between these two nested structures: at each level  $\ell$ , for  $\ell = 0, 1, \dots, N-1$ , we iteratively select the basis functions from the underlying spline space  $V^\ell$  which act only on the current domain  $\Omega^\ell$ , i.e., whose support is contained in  $\Omega^\ell$ . At the same time we discard from the hierarchical basis the basis functions selected in the earlier steps which act only on  $\Omega^\ell$ . The local action of the refinement procedure is then immediately guaranteed by construction. Moreover, the local linear independence is inherited from the underlying B-spline bases.

The selection mechanism for the definition of a hierarchical B-splines basis introduced by Kraft [12] by means of subsequent dyadic refinements ensures that

- hierarchical basis functions allows proper local refinement and are linearly independent [12, Theorem 1],
- the hierarchical B-spline basis is *weakly* stable, i.e. the stability constants have at most a polynomial growth in the number of hierarchical levels [12, Theorem 3].

Hierarchical B-splines have already been applied in several applications related to geometric modeling — see for example [8, 9, 10]. In addition, a hierarchical quasi-interpolant together with approximation algorithms and scattered data approximation and interpolation problems were also discussed in [12]. A more detailed analysis of the above mentioned topics can be found in [13]. The case of partly overlapping boundaries of the sub-domains which are selected for further refinement and the application of hierarchical B-splines in isogeometric analysis have recently been considered in [24].

## 1.2 Contributions and outline

The goal of the present paper is to investigate dimensions and bases of hierarchical tensor-product B-spline spaces. The starting point of our study is a generalization of the dimension results for bivariate tensor-product polynomial spline spaces to multi-cell domains. When considering tensor-product spline functions with maximum order of smoothness, it turns out that the dimension formula on domains whose boundaries are piecewise linear curves (which satisfy a specific reasonable assumption) can be derived from the standard one related to rectangular grids (see, e.g., [19]) by including certain correction factors.

Under certain mild assumptions on the multi-cell domain considered at each level, the dimension of the above mentioned space is equal to the number of B-splines defined on the corresponding grid and which effectively act on it. This computation is then used to construct a basis for the space of bivariate tensor-product splines on multi-grid multi-cell domains, i.e., on hierarchies of multi-cell domains. This allows us to conclude that the classical hierarchical B-spline basis is indeed a basis for the considered spline space. *Consequently, the span of the hierarchical B-spline basis contains all spline functions of given bi-degree  $(d, d)$  and maximal smoothness that exist on the underlying hierarchical grid.*

The structure of the paper is as follows.

Section 2 reviews the notion of hierarchical B-splines and introduces tensor-product splines on multi-cell domains and on multi-grid multi-cell domains. It also provides a detailed overview of the subsequent analysis.

The next two sections study tensor-product splines on multi-cell domains. Section 3 derives the dimension result for the space of tensor-product splines of bi-degree  $(d, d)$  with maximum order of smoothness defined on a multi-cell domain. Subsequently, Section 4 identifies the assumptions concerning the cell configuration that are needed to guarantee that the set of B-splines which act on this set of cells is a basis for the spline space defined on it.

Section 5 uses these observations in order to obtain results on dimensions and bases for tensor-product splines, with the same smoothness properties as before, defined on multi-grid multi-cell domains. Finally, Section 6 concludes the paper.

## 2 Preliminaries

We start by revisiting the construction of hierarchical B-splines. We also describe the overall structure of the proposed analysis.

### 2.1 Hierarchical B-splines

Let  $\{V^\ell\}_{\ell=0,\dots,N-1}$  be a sequence of  $N$  nested tensor-product spline spaces so that

$$V^\ell \subset V^{\ell+1},$$

for  $\ell = 0, \dots, N - 2$ . We assume the bi-degree and smoothness at each level  $\ell$  equal to  $(d, d)$  and  $(d - 1, d - 1)$ , respectively.

Each spline space  $V^\ell$  is spanned by a tensor-product B-spline basis  $T^\ell$  defined on the two knot sequences  $X^\ell = \{x_i^\ell\}_{i=0,\dots,p(\ell)}$  and  $Y^\ell = \{y_j^\ell\}_{j=0,\dots,q(\ell)}$  containing the horizontal and vertical knots, respectively. These knot sequences, defined by only single knots at all levels, are also nested. Consequently, each space  $V^\ell$  has an associated grid

$$G^\ell = \{(x_{i-1}^\ell, x_i^\ell) \times (y_{j-1}^\ell, y_j^\ell) : i = 1, \dots, p(\ell), j = 1, \dots, q(\ell)\}$$

consisting of cells (axis-aligned boxes) such that the restriction of  $f \in V^\ell$  to any of these cells is a tensor-product polynomial of bi-degree  $(d, d)$ .

We may observe that, in our case of only single knots at all levels, the support of any B-spline always consists of  $(d + 1) \times (d + 1)$  elementary cells of the parametric grid. If  $d$  is even, we can then identify each basis function with the central elementary cell of its support. When  $d$  is odd, instead, we may identify each basis function with the center of its support. These naive *anchors* are called *odd* and *even* depending on the bi-degree. They are shown in Figure 1 for the first four low bi-degree cases.

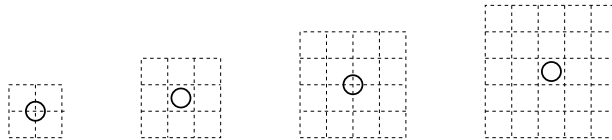


Figure 1: Basis functions representation in terms of odd ( $d = 1, 3, \dots$ ) and even ( $d = 2, 4, \dots$ ) anchors. From left to right:  $d = 1, 2, 3, 4$ .

In addition, we consider a finite sequence of  $N$  nested bounded open sets  $\{\Omega^\ell\}_{\ell=0,\dots,N-1}$  so that

$$\Omega^\ell \supseteq \Omega^{\ell+1}, \tag{1}$$

for  $\ell = 0, \dots, N - 1$ , with  $\Omega^N = \emptyset$ . At each level the boundary  $\partial\Omega^\ell$  is aligned with the knot lines of  $V^{\ell-1}$ ,  $\ell = 1, \dots, N - 1$ , while  $\partial\Omega^0$  is aligned with the knot lines of  $V^0$ . Moreover, we assume that

$$\Omega^0 \subseteq [x_d^0, x_{p(0)-d}^0] \times [y_d^0, y_{q(0)-d}^0].$$

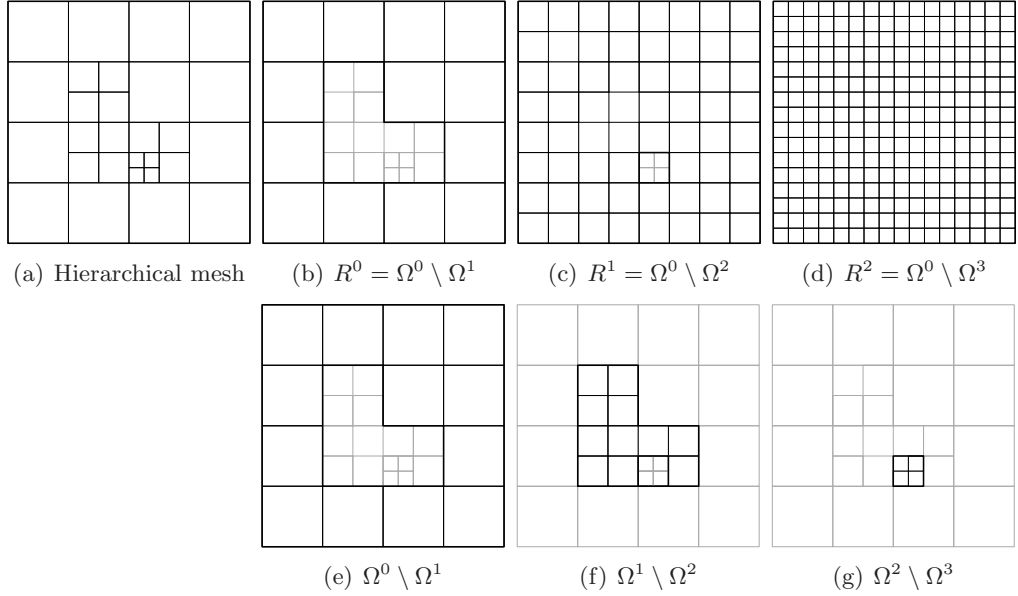


Figure 2: The hierarchical mesh defined by restricting the grid of  $V^\ell$  to  $\Omega^\ell$  for  $\ell = 0, \dots, 3$ , where  $\Omega^3 = \emptyset$  (a), the rings  $R^\ell$  (b-d) and the differences  $\Omega^\ell \setminus \Omega^{\ell+1}$  (e-g).

and we consider the support of any function  $f$  when restricted to the domain  $\Omega^0$  by defining

$$\text{supp } f = \{(x, y) : f(x, y) \neq 0 \wedge (x, y) \in \Omega^0\}.$$

This modified support enables suitable refinements also along the boundaries of  $\Omega^0$ .

The domain  $R^\ell = \Omega^0 \setminus \Omega^{\ell+1}$  will be called a *ring* — even if it may not be ring-shaped — because, conceptually, it represents  $\Omega^0$  with a *hole* given by  $\Omega^{\ell+1}$ . In order to describe this set, we first represent  $\Omega^0$  with respect to the grid of  $V^\ell$  and then delete the cells that belong to  $\Omega^{\ell+1}$ . Consequently,  $R^\ell$  consists of *cells with respect to the tensor-product grid of level  $\ell$* . We shall refer to such a set — along with the corresponding grid structure — as a *multi-cell domain*, see Figure 2.

When considering the difference  $\Omega^\ell \setminus \Omega^{\ell+1}$  of the adjacent domains in the domain hierarchy, we find another sequence of multi-cell domains, consisting of mutually disjoint sets. Their union — along with the corresponding grid structures — will be called a *multi-grid multi-cell domain*, see again Figure 2.

The following definition generalizes the hierarchical B-spline basis originally introduced by Kraft in [12], where, for any hierarchical level, only sub-domains with disjoint boundaries defined as union of B-splines supports of the previous level were considered.

**Definition 1.** *The hierarchical basis  $\mathcal{K}$  is defined as*

$$\mathcal{K} = \bigcup_{\ell=0}^{N-1} \mathcal{K}^\ell$$

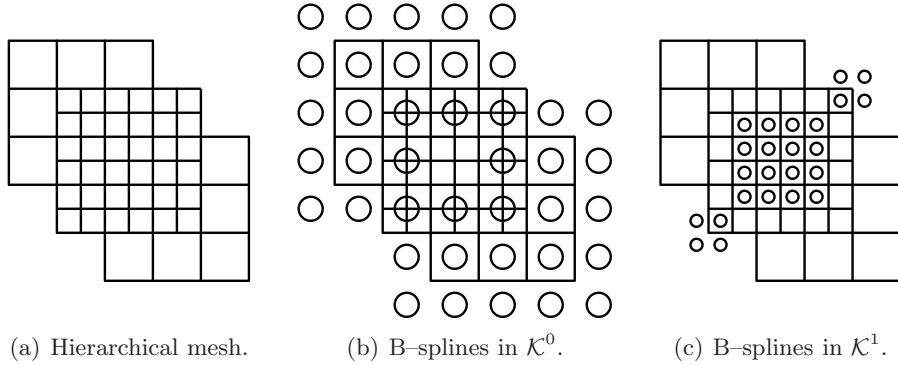


Figure 3: Left: an example of a hierarchical mesh which represents a multi-grid multi-cell domain consisting of two multi-cell domains. Center and right the corresponding hierarchical bi-quadratic B-spline basis  $\mathcal{K}$  which contains basis functions (represented by their anchors) from  $T^0$  and  $T^1$ .

with

$$\mathcal{K}^\ell = \{\tau \in T^\ell : \text{supp } \tau \cap R^{\ell-1} = \emptyset \wedge \text{supp } \tau \cap R^\ell \neq \emptyset\} \quad (2)$$

where  $T^\ell$  is the tensor-product B-spline basis of the space  $V^\ell$  as described in the beginning of this section. We define  $R^{-1} = \emptyset$  to include the case  $\ell = 0$ .

An example is shown in Figure 3.

At each level  $\ell$ , except for functions in  $\mathcal{K}^k$  with  $k < \ell$  which belong to coarser levels, only the basis functions in  $\mathcal{K}^\ell$  are non-zero on  $\Omega^\ell \setminus \Omega^{\ell+1}$ . In view of the local linear independence of B-splines, one can use this observation to prove the linear independence of the basis  $\mathcal{K}$  [12, 24].

## 2.2 Overview

We consider the spaces of bivariate tensor-product splines on the multi-cell domains  $R^\ell$ ,

$$S^\ell = \left\{ f \in \mathcal{C}^{d-1, d-1}(R^\ell) : f|_C \in \Pi^{d, d}(C) \forall C \in G^\ell, C \subseteq R^\ell \right\}, \quad (3)$$

where we denote by  $\Pi^{d, d}(P)$  the space of polynomial functions of bi-degree  $(d, d)$  over  $P \subset \mathbb{R}^2$ . The space  $S^\ell$  consists of all piecewise polynomial functions of bi-degree  $(d, d)$  on the subdivision of the plane which is obtained by restricting the grid of  $V^\ell$  to  $R^\ell$  for a fixed value of  $\ell$ .

The analysis of dimensions and bases of these spaces will prepare us for analyzing the space of bivariate tensor-product splines on a multi-grid multi-cell domain,

$$W = \left\{ f \in \mathcal{C}^{d-1, d-1}(\Omega^0) : f|_{R^\ell} \in S^\ell \forall \ell = 0, \dots, N-1 \right\}. \quad (4)$$

The space  $W$  consists of all piecewise polynomial functions of bi-degree  $(d, d)$  on the subdivision of the plane which is obtained by restricting the grid of  $V^\ell$  to  $\Omega^\ell$  for  $\ell = 0, \dots, N - 1$ .

We identify some restrictions on the hierarchical grid defined by the nested sequence of domains  $\Omega^\ell$  along with the associated spaces  $V^\ell$  which imply that the set of hierarchical B-splines constructed according to Definition 1 forms a basis of  $W$ . The strategy of our analysis can be summarized as follows.

- Section 3 studies the space  $S^\ell$  of tensor-product splines on a multi-cell domain and proposes a construction based on integrations which generates any function in  $S^\ell$  from a suitable set of characteristic data, consisting of residual and boundary values. Conversely, from any function in  $S^\ell$  one can easily derive the corresponding set of characteristic data. By carefully analyzing the dependencies between the boundary values we compute the dimension  $D^\ell$  of the space  $S^\ell$ .
- Then, by introducing the definition of the *offset* to a domain and of its *length*, we can formulate an assumption which the ring  $R^\ell$  has to satisfy so that the number of B-spline functions of level  $\ell$  acting on  $R^\ell$  is equal to  $D^\ell$  (Section 4). The assumption is needed to guarantee that B-splines whose support intersect opposite sides along the boundaries of the domain do not overlap each other.
- Finally, by iteratively using the earlier results, Section 5 shows that hierarchical B-splines form a basis of the space  $W$  of tensor-product splines on multi-grid multi-cell domains, see (4), provided that the assumptions regarding the cell configurations are satisfied at each level.

### 3 Dimension of splines on multi-cell domains

In this section we study the dimension of the space of bivariate tensor-product splines  $S^\ell$  introduced in (3) on the ring  $R^\ell$  for a fixed value of  $\ell$ .

We describe a sequence of  $2d$  differentiations, first in the vertical and then in the horizontal direction, which allow to associate a set of *boundary data* to each function  $f \in S^\ell$ , simply by restricting the obtained derivatives to some of the domain boundaries. Moreover, we define *residual data* by evaluating the partial derivative of order  $(d, d)$  (which is a piecewise constant function) at the cells that form the domain.

Conversely, any such function  $f$  can be recovered from these data via integrations. The residual data defines the initial function, and the boundary data serve as boundary values for the  $2d$  integrations.

We perform a detailed analysis to enumerate the degrees of freedom related to the bottom boundary, which is subdivided in *maximum horizontal components*. These components are then suitably connected together to construct *feasible characteristic data* for the differentiation and integration processes. The analysis leads to a dimension result for the space  $S^\ell$ .

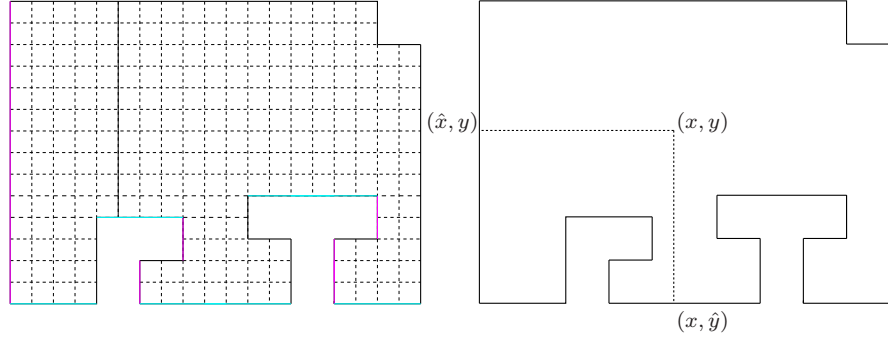


Figure 4: The ring  $R^\ell = \Omega^0 \setminus \Omega^{\ell+1}$ , its grid, and the point sets  $L$  and  $B$  composed of all the left and bottom edges (magenta and cyan lines, respectively, on the left). The identification of  $\hat{x} = \hat{x}(x, y)$  and  $\hat{y} = \hat{y}(x, y)$  introduced in the proof of Proposition 4 is also shown (right).

### 3.1 Residual and boundary data

Given a fixed level  $\ell$ , we consider the space  $S^\ell$  as defined by (3). By introducing the notions of *characteristic* and *feasible* data, we identify the isomorphism between the spline space  $S^\ell$  and the space of feasible characteristic data related to  $R^\ell$ .

Assuming to sweep the domain with a horizontal line starting from the up-most horizontal boundary line, the *bottom segments* are the horizontal segments along the boundary which mark the domain from below, i.e., the inner part of the domain is above these segments. Analogously, assuming to sweep the domain with a vertical line starting from the rightmost vertical boundary line, the *left edges* are the vertical segments along the boundary which mark the domain from the left, i.e., the inner part of the domain is on the right of these segments. We denote by  $B$  and  $L$  the point sets composed of all the bottom and left edges which belong to  $R^\ell$  (see Figure 4).

Let  $B_1, \dots, B_h$  and  $L_1, \dots, L_v$  be the horizontal and vertical elementary segments in which the bottom and left boundaries of the domain are subdivided. The bottom and left edges  $B$  and  $L$  can then be expressed as

$$B = \bigcup_{i=1}^h B_i, \quad L = \bigcup_{j=1}^v L_j.$$

**Definition 2.** Denoting by  $\Pi^{d,d}(P)$  the space of polynomial functions of bi-degree  $(d, d)$  over  $P \subset \mathbb{R}^2$ , we say that

$$F = (b_1, \dots, b_d, l_1, \dots, l_d, r)$$

where

$$b_k : B \rightarrow \mathbb{R}, \quad l_k : L \rightarrow \mathbb{R}, \quad r : R^\ell \rightarrow \mathbb{R},$$

with  $k = 1, \dots, d$ , so that, for all  $i = 1, \dots, h, j = 1, \dots, v$  and for each cell  $C$  of the grid of  $R^\ell$ ,

$$b_k \Big|_{B_i} \in \Pi^{d,0}(B_i), \quad l_k \Big|_{L_j} \in \Pi^{0,0}(L_j), \quad \text{and} \quad r \Big|_C \in \Pi^{0,0}(C),$$

is a vector of **characteristic data**.

Note that the boundary data  $b_k(x, y)$  are *piecewise polynomials in  $x$*  evaluated on the bottom horizontal edge segments. As it will be detailed later, a smoothness of order  $d - 1$  has to be required also across *jumps* along the bottom boundary.

The boundary data  $l_k(x, y)$  are *piecewise constant functions* associated to the left vertical edge segments. Finally, the residual data  $r(x, y)$  specifies a *constant real value* for each cell that belongs to the grid of  $R^\ell$ .

A vector  $F$  of *characteristic data* is obtained from a function  $f \in S^\ell$  by means of the characteristic operator  $\mathcal{M}$  as

$$F = \mathcal{M}(f) = (b_1, \dots, b_d, l_1, \dots, l_d, r)$$

where

$$\begin{aligned} b_1(x, y) &= f(x, y) \Big|_B, & l_1(x, y) &= \frac{\partial^d}{\partial y^d} f \Big|_L \\ b_2(x, y) &= \frac{\partial}{\partial y} f(x, y) \Big|_B, & l_2(x, y) &= \frac{\partial}{\partial x} \frac{\partial^d}{\partial y^d} f \Big|_L \\ &\vdots & &\vdots \\ b_d(x, y) &= \frac{\partial^{d-1}}{\partial y^{d-1}} f(x, y) \Big|_B, & l_d(x, y) &= \frac{\partial^{d-1}}{\partial x^{d-1}} \frac{\partial^d}{\partial y^d} f \Big|_L, \end{aligned}$$

and

$$r(x, y) = \frac{\partial^d}{\partial x^d} \frac{\partial^d}{\partial y^d} f(x, y) \Big|_C \quad \text{for each cell } C \text{ of the grid of } R^\ell.$$

**Definition 3.** A vector  $F$  of characteristic data is said to be **feasible** if there exists  $f \in S^\ell$  such that  $F = \mathcal{M}(f)$ .

Clearly, the set of feasible characteristic data forms a linear space. We can then relate this space to the spline space  $S^\ell$  by means of the following proposition.

**Proposition 4.** The mapping  $\mathcal{M} : S^\ell \rightarrow F$  between the spline space and the space of feasible characteristic data is an isomorphism of linear spaces.

*Proof.* For any point  $(x, y) \in R^\ell$ , consider the rays with directions  $(-1, 0)$  and  $(0, -1)$  and let  $\hat{x} = \hat{x}(x, y)$ ,  $\hat{y} = \hat{y}(x, y)$  be the horizontal and vertical coordinate of the intersection of these rays with the first vertical/horizontal boundary edge reached by them (see Figure 4). We can relate a function  $f$  in  $S^\ell$  and a vector  $F$  of characteristic data

in terms of the following differentiation/integration process. First, we execute  $d$  vertical differentiations

$$\begin{aligned}
f(x, y) &= b_1(x, \hat{y}) + \int_{\hat{y}}^y \frac{\partial}{\partial y} f(x, \eta) d\eta, \\
\frac{\partial}{\partial y} f(x, y) &= b_2(x, \hat{y}) + \int_{\hat{y}}^y \frac{\partial^2}{\partial y^2} f(x, \eta) d\eta, \\
&\vdots \\
\frac{\partial^{d-1}}{\partial y^{d-1}} f(x, y) &= b_d(x, \hat{y}) + \int_{\hat{y}}^y \frac{\partial^d}{\partial y^d} f(x, \eta) d\eta,
\end{aligned} \tag{5}$$

where  $\hat{y}$  depends on  $(x, y)$ , i.e.,  $\hat{y} = \hat{y}(x, y)$ . Then, we continue with  $d$  horizontal differentiations

$$\begin{aligned}
\frac{\partial^d}{\partial y^d} f(x, y) &= l_1(\hat{x}, y) + \int_{\hat{x}}^x \frac{\partial}{\partial x} \frac{\partial^d}{\partial y^d} f(\xi, y) d\xi, \\
\frac{\partial}{\partial x} \frac{\partial^d}{\partial y^d} f(x, y) &= l_2(\hat{x}, y) + \int_{\hat{x}}^x \frac{\partial^2}{\partial x^2} \frac{\partial^d}{\partial y^d} f(\xi, y) d\xi, \\
&\vdots \\
\frac{\partial^{d-1}}{\partial x^{d-1}} \frac{\partial^d}{\partial y^d} f(x, y) &= l_d(\hat{x}, y) + \int_{\hat{x}}^x r(\xi, y) d\xi,
\end{aligned} \tag{6}$$

where  $\hat{x}$  depends on  $(x, y)$ , i.e.,  $\hat{x} = \hat{x}(x, y)$ . Hence, starting from a function  $f \in S^\ell$ , we may identify the associated feasible characteristic data  $F$  simply by means of Definition 3. On the other hand, starting with the set of constant values  $r(x, y)$ , which represent the derivative of order  $d$  in both directions, and with the following partial derivatives defined by the functions  $b_1, \dots, b_d$  and  $l_1, \dots, l_d$ , we can reconstruct  $f$  by executing the above mentioned sequence of integrations in reverse order.  $\square$

**Remark 5.** *The asymmetry of Definition 2 is related to the order of execution of the sequence of differentiations introduced in the proof of Proposition 3. Alternative sequences of differentiations may be considered also, which will lead to similar results, but requiring different assumptions about the cell configuration (cf. Assumption 1 on page 14).*

### 3.2 Maximum horizontal components

We now need to specify the continuity conditions that a subset of characteristic data has to satisfy in order to be properly associated with a function  $f$  in  $S^\ell$  by the mapping  $\mathcal{M}$  as described in the previous Lemma. We may observe that the functions  $b_1, \dots, b_d$  are inter-dependent connected to each other, while the constants  $l_1, \dots, l_d$  are not. This difference is due to the non-symmetric order of the differentiations.

In order to properly identify the required connections between the boundary data  $b_k$ , we need to detail the analysis by further decomposing the bottom boundary:

**Definition 6.** A connected horizontal component (HC) is a component of the bottom boundary composed of adjacent horizontal segments connected by only vertical edges. It is said to be a maximum HC (MHC) if it is not contained in any other HC.

Each horizontal pair of adjacent elementary segments which belong to any MHC of the considered domain can be joined together according to one of the three cases shown in Figure 5 and indicated as flat join, step up join, and step down join.

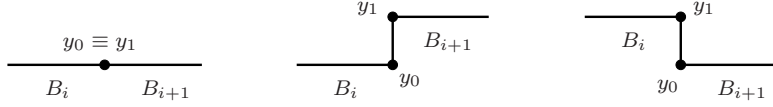


Figure 5: Joins between adjacent elementary segments: flat join (left), step up join (center), and step down join (right).

For any function  $b_1, \dots, b_d$ , we may require the needed continuity in all the inner connection points of each MHC as a  $C^{d-1}$  join between

$$b_k \Big|_{B_i} + v_k^i \quad \text{and} \quad b_k \Big|_{B_{i+1}} + u_k^{i+1} \quad \text{at} \quad \pi(B_i) \cap \pi(B_{i+1}),$$

for  $i = 1, \dots, h - 1$ , where

$$v_k^i = 0, \quad u_k^i = 0, \quad \text{in case of a flat join,} \quad (7)$$

$$v_k^i = \int_{y_0}^{y_1} \frac{\partial^{k-1}}{\partial y^{k-1}} f(x, \eta) d\eta, \quad u_k^i = 0, \quad \text{in case of a step up join,} \quad (8)$$

$$v_k^i = 0, \quad u_k^i = \int_{y_0}^{y_1} \frac{\partial^{k-1}}{\partial y^{k-1}} f(x, \eta) d\eta, \quad \text{in case of a step down join.} \quad (9)$$

All polynomials are independent of  $y$  and are considered as functions of  $x$  only. The symbol  $\pi$  denotes the projection onto the  $x$ -axis, i.e.,  $\pi(x, y) = x$ .

The contribution – in terms of degrees of freedom – of all the MHCs which composed the bottom boundary of the given domain is then specified in the following Lemma.

**Lemma 7.** The number of degrees of freedom associated with an MHC composed of  $e$  elementary horizontal segments is  $d(e + d)$ .

*Proof.* For any function  $b_k$ ,  $k = 1, \dots, d$ ,

$$b_k \Big|_{B_1} + v_k^1 \quad \text{has to have a } C^{d-1} \text{ joint with } b_k \Big|_{B_2} + u_k^2 \quad \text{at} \quad \pi(B_1) \cap \pi(B_2),$$

$$b_k \Big|_{B_2} + v_k^2 \quad \text{has to have a } C^{d-1} \text{ joint with } b_k \Big|_{B_3} + u_k^3 \quad \text{at} \quad \pi(B_2) \cap \pi(B_3),$$

and so on until

$$b_k \Big|_{B_{e-1}} + v_k^{e-1} \quad \text{and} \quad b_k \Big|_{B_e} + u_k^e \quad \text{at} \quad \pi(B_{e-1}) \cap \pi(B_e),$$

where  $u_k^i, v_k^i$  are defined by (7)–(9) for  $i = 1, \dots, e$ . Since these relations only involve polynomial functions over the elementary segments  $B_1, \dots, B_e$ , by using polynomial extrapolations we can equivalently express the above smoothness conditions as

$$c_k^{i-1} \text{ has to have a } C^{d-1} \text{ joint to } c_k^i \text{ at } \pi(B_{i-1}) \cap \pi(B_i)$$

for  $i = 1, \dots, e$ , where

$$c_k^i = b_k \Big|_{B_i} + \sum_{s=1}^{i-1} (u_k^{s+1} - v_k^s).$$

Hence,  $(c_k^i)_{i=1, \dots, e}$  form a  $C^{d-1}$  polynomial spline which is well-known to possess  $e + d$  degrees of freedom.  $\square$

### 3.3 Construction of feasible characteristic data

In order to extend the count of the number of degrees of freedom associated to a single MHC to the entire bottom boundary of  $R^\ell$ , we now investigate how different maximum horizontal components influence each other. The following three types of MHCs (see also Figure 6) exist:

- (a) MHC not subject to boundary conditions;
- (b) MHC with one boundary condition (on its left-hand or right-hand side);
- (c) MHC with two boundary conditions.

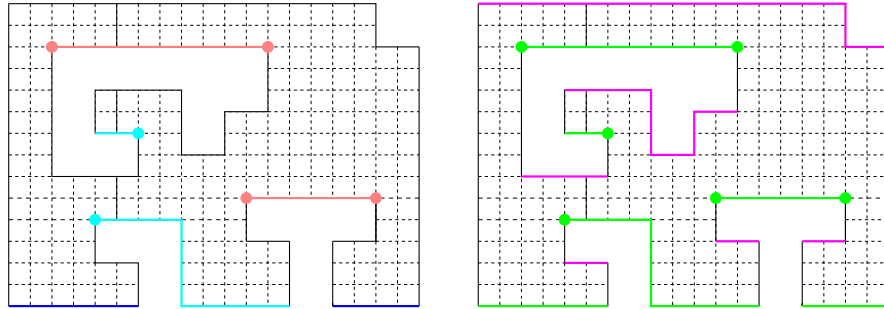


Figure 6: Classification of horizontal components: MHC not subject to boundary conditions (blue lines on the left), MHC with one boundary condition (cyan lines on the left), MHC with two boundary conditions (pink lines on the left). Also shown is the distinction between upper and lower MHCs (in magenta and green, respectively, on the right) introduced in Lemma 11.

We may observe that we can always split the bottom boundary of the domain in a unique sequence of MHCs. Moreover, as outlined by the following Lemma, at least one of the MHCs in this sequence is not subject to boundary conditions when considered

in the vertical integration process described in the proof of Lemma 4. We will indicate an MHC of this type as *independent*. An independent MHC is obviously *left free* (no boundary conditions on left side) and *right free* (no boundary conditions on right side).

**Lemma 8.** *There always exists at least one independent MHC in the bottom boundary of the domain.*

*Proof.* Assume that no MHC is both left and right free. The leftmost corner of the bottom boundary of the domain is necessarily left free. Since the corresponding leftmost MHC cannot be also right free, the second leftmost MHC along the bottom boundary of the domain is also left free. Again, this second MHC cannot be also right free. We may then continue until we arrive at the rightmost MHC along the bottom boundary. However, this last MHC is necessarily also right free. This contradicts our assumption hence the proof is complete.  $\square$

An independent MHC imposes boundary conditions on other MHCs and its *shadow* (see Figure 7) decreases the domain. We are then able to describe a recursive algorithm to define feasible characteristic data for the integration process described in the proof of Lemma 4. We start from any of the independent MHCs which are present in the the considered domain. In view of the previous Lemma, at least one of them always exists.

**Algorithm 9.**

*Input:* a domain  $\Omega$ , a constant value  $r$  for each cell of  $\Omega$ , the functions  $l_k$ ,  $k = 1, \dots, d$ , on the vertical edges of the left boundary of  $\Omega$ .

1. Evaluate, via equations (6),

$$\frac{\partial^{d-1}}{\partial x^{d-1}} \frac{\partial^d}{\partial y^d} f(x, y), \quad \dots, \quad \frac{\partial}{\partial x} \frac{\partial^d}{\partial y^d} f(x, y), \quad \frac{\partial^d}{\partial y^d} f(x, y);$$

2. let  $\Omega$  be the initial sub-domain not subject to boundary conditions;
3. select an independent MHC with respect to the current sub-domain;
4. for  $k = d, \dots, 1$ 
  - (a) choose  $b_k$  on the selected MHC by taking into account possible boundary conditions of adjacent sub-domains (see below),
  - (b) evaluate, via equations (5),

$$\frac{\partial^{k-1}}{\partial y^{k-1}} f(x, y),$$

in its shadow and determine boundary conditions on adjacent MHCs which will be considered by neighboring sub-domains – see Figure 7;

5. reduce/split the current sub-domain by deleting the shadow of the selected MHC. This gives a set of sub-domains;

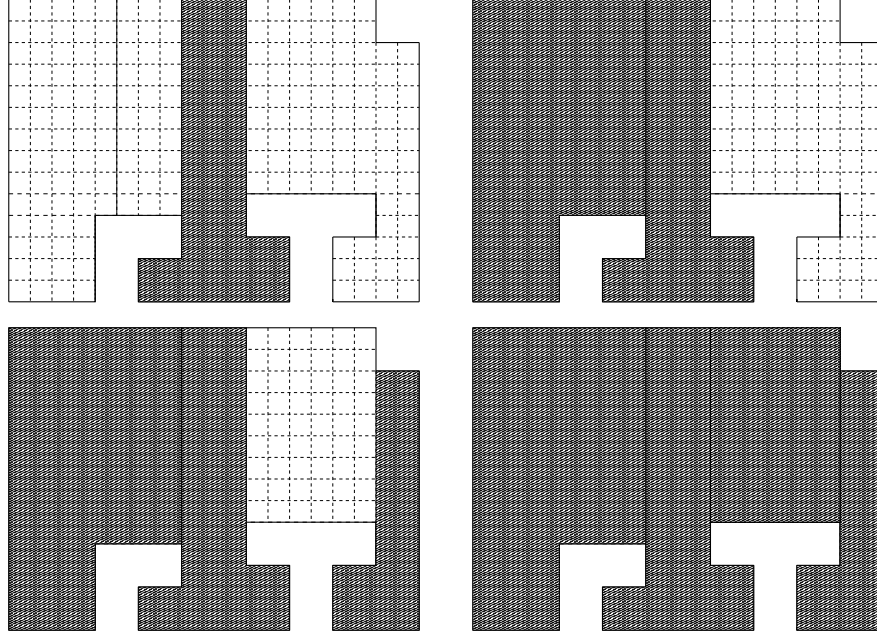


Figure 7: Boundary conditions computation with Algorithm 9. At each step the shadow of the selected independent MHC decreases and possibly also splits the domain.

6. if the set of sub-domains is not empty then apply recursively step 3–5 to each sub-domain identified in step 5<sup>1</sup>.

*Output:* a set of feasible characteristic data and a corresponding spline function  $f$  on  $\Omega$ .

We may observe that, for any MHC composed of  $e$  horizontal elementary segments, we have  $e + d$  degrees of freedom (see the proof of Lemma 11 for the details). To impose the smoothness conditions as required by the integration process described above, when we consider an MHC with 2 boundary conditions, we have  $e + d$  degrees of freedom minus a term of  $2d$  given by the left and right boundary conditions. This leads to  $e - d$  degrees of freedom, and then the length  $e$  of the MHC has to be greater or equal to  $d$ . We are then led to formulate the following assumption.

**Assumption 1.** *The length (number of elementary horizontal segments) of any lower maximum horizontal component with two boundary conditions is at least  $d$ .*

We summarize the results of this section:

**Lemma 10.** *If Assumption 1 is satisfied, Algorithm 9 gives feasible characteristic data (boundary conditions) for the integration process described in the proof of Lemma 4.*

This can be proved easily by analyzing Algorithm 9.

---

<sup>1</sup>The values obtained in step 4 are used as boundary conditions on the remaining sub-domains.

### 3.4 Dimension formula

By using the previous analysis on the compatibility conditions between maximum horizontal components, we can derive the dimension of the spline space  $S^\ell$  in terms of the number of cells of  $R^\ell$ , the number of cells along its perimeter, the number of its connected components, and the number of holes. After analyzing the case of multi-cell domains without holes, we generalize the result to domains possessing one or more holes.

By firstly assuming the absence of holes, in view of the previous analysis, the bottom boundary is composed of:

1. one MHC of type (a), i.e., no boundary conditions – this is the one that, according to Lemma 8, always exists,
2. an arbitrary number of type (b) MHCs, i.e., one boundary condition,
3. a remaining arbitrary equal number of type (a) and (c) MHCs, i.e., zero and two boundary conditions, respectively.

Hence, the invariant property of the bottom boundary is that for each (c) there is always an (a). Let  $h_i$  be the number of elementary horizontal segments that compose one MHC. In the case of an MHC of type (a), the considered horizontal component contributes  $h_i + d$  degrees of freedom, while in case (b) we have to consider the  $d$  conditions to obtain a  $C^{d-1}$  join on its left or right boundary, leading to  $h_i + d - d = h_i$ . In case (c), instead, we have to take into account the  $d$  conditions to obtain a  $C^{d-1}$  join both on the left and right boundary of the MHC, leading to  $h_i + d - 2d = h_i - d$ . The total number of degrees of freedom associated with the bottom boundary of the domain is then always  $\sum h_i + d$ , as confirmed by the following Lemma.

**Lemma 11.** *Let  $M$  be the number of connected components of  $R^\ell$ . If the considered domain does not exhibit holes, each one of the  $d$  vertical integrations contributes*

$$\# \text{ of horizontal segments} + Md$$

*degrees of freedom.*

*Proof.* We consider upper MHC and lower MHC (UMHC and LMHC) as shown on the right of Figure 6, and assume that the boundary is oriented counterclockwise. UMHC and LMHC alternate along the boundary. Between neighboring MHC, the boundary makes either a left turn or a right turn, both by 180 degrees. The total number of left turns is equal to the total number of right turns plus  $2M$ , because the boundary of any connected components of  $R^\ell$  is a simple closed curve and the rotation index is therefore 1. We may observe that, if a LMHC follows

- a left turn, then there is no boundary condition on the left-hand side;
- a right turn, then there is one.

On the other hand, if a LMHC is followed by

- a left turn, then there is no boundary condition on its right-hand side;
- a right turn, then there is one.

For a LMHC with  $h_i$  edges, we have  $(d+1)h_i - d(h_i - 1) = h_i + d$  degrees of freedom. If we have  $t$  LMHC, then will have  $2t$  left turns or right turns, hence we have  $t + M$  left turns and  $t - M$  right turns. Each right turn imposes one boundary condition, hence it reduces the number of degrees of freedom by  $d$ . Summing up, we get

$$\sum_{i=1}^t (h_i + d) - (t - M)d = \sum_{i=1}^t h_i + td - td + Md = \sum_{i=1}^t h_i + Md$$

degrees of freedom. □

To relax the restriction related to the absence of holes and analyze how this influences the number of available degrees of freedom, we assume the boundaries of the holes are oriented counterclockwise as we already did for the boundary of the domain. Since the outer boundary of the hole is obviously inside the parametric domain, the distinction between lower and upper maximum connected horizontal component is now reversed – see again Figure 6. This implies that, in this case, a left turn before or after an MHC is the one which imposes a boundary condition on the left-hand side or right-hand side of the considered horizontal component.

For an LMHC with  $h_i$  edges, we have  $(d+1)h_i - d(h_i - 1) = h_i + d$  degrees of freedom as before. Again if we have  $t$  LMHC, then will have  $2t$  left turns or right turns, hence we have  $t + 1$  left turns and  $t - 1$  right turns. Each left turn imposes one boundary condition, hence it reduces the number of degrees of freedom by  $d$ . Summing up we get

$$\sum_{i=1}^t (h_i + d) - (t + 1)d = \sum_{i=1}^t h_i + td - td - d = \sum_{i=1}^t h_i - d$$

degrees of freedom.

**Remark 12.** *If the considered domain is characterized by one or more holes, for each of the  $d$  vertical integrations, any hole reduces the total degrees of freedom by  $d$ .*

**Theorem 13.** *If Assumption 1 is satisfied, the dimension of the space  $S^\ell$  is given by*

$$D^\ell = c + \frac{p}{2}d + Md^2 - Hd^2, \quad (10)$$

where  $c$  is the number of cells of the domain,  $p$  the number of cells along its perimeter,  $M$  the number of connected components of the domain, and  $H$  the number of holes.

*Proof.* The first contribution simply arises from the  $c$  constant values for  $r(x, y)$  that we associate to each cell of the considered domain. For each left edge considered in the  $d$  horizontal integrations, the involved partial derivatives  $l_1, \dots, l_d$  are constant with respect to the variable  $y$ . This leads to  $d$  times one degree of freedom for each vertical segment on the left boundary. The contribution to the available degrees of freedom

which arises from the  $d$  vertical integrations is slightly more involved. However, we know from the previous analysis that is equal to  $d(h + Md - Hd)$  for a domain with  $M$  connected components and  $H$  holes. We may then conclude that the dimension of the space generated by the set of feasible characteristic data is

$$c + d(v + h + Md - Hd) = c + d\frac{p}{2} + Md^2 - Hd^2,$$

which directly leads to (10).  $\square$

- Remark 14.**
1. When  $M = 1$  and  $H = 0$ , the value of  $D^\ell$  in (10) reduces to the dimension of bivariate tensor-product splines, defined by only single knots, on a rectangular grid, namely  $D^\ell = (h + d)(v + d) = hv + (h + v)d + d^2 = c + \frac{p}{2}d + d^2$ .
  2. The techniques developed in [17], which discusses dimensions of spline spaces on  $T$ -subdivisions of a rectangular domain without holes, should give the same dimension formula (10) provided that each edge segment contains at least  $d + 1$  nodes.
  3. By using a slightly different algorithm for constructing the boundary conditions it is possible to formulate a weaker assumption which still implies the dimension formula of Theorem 13. It suffices to assume that the horizontal width of each hole is at least  $d$  segments. However, this would not improve the final result in Theorem 20.

## 4 Tensor-product spline bases on multi-cell domains

In this section we prove that the number of tensor product B-splines of bi-degree  $(d, d)$  defined by only single knots in both directions, whose support overlaps a given domain, is equal to the dimension  $D^\ell$  in (10). We focus again on the multi-cell domain  $R^\ell = \Omega^0 \setminus \Omega^{\ell+1}$  for a fixed level  $\ell$ .

To formulate the condition that the considered domain has to satisfy so that B-splines whose support intersect opposite sides along its boundaries do not overlap each other, we begin by introducing the notion of the *offset* to a domain. Subsequently, the assumptions on the domain configuration and the enumeration of B-splines acting on  $R^\ell$  are discussed.

### 4.1 Offset to a domain

Considering the cells which belong to the grid  $G^\ell$  associated with the space  $V^\ell$ , let  $R_k^\ell$  be the *offset region* at distance  $k$  to  $R^\ell$ . More precisely,  $R_0^\ell$  consists of all cells which are contained in  $R^\ell$ ,

$$R_0^\ell = \{C \in G^\ell : C \subseteq R^\ell\},$$

and the remaining offset regions  $R_{k+1}^\ell$  are obtained by collecting the cells along the outer boundary of  $R_k^\ell$ ,

$$R_{k+1}^\ell = \{C \in G^\ell : \overline{C} \cap \overline{\partial R_k^\ell} \neq \emptyset \wedge (\forall_{j=0}^k : C \cap R_j^\ell = \emptyset)\}.$$

We introduce the definitions of the *offset curve* to the ring  $R^\ell$  at a certain distance and of its *length*.

**Definition 15.** *The offset curve to the ring  $R^\ell$  is the piecewise linear curve defined as follows.*

(I)  $C_0$ , the offset curve at distance 0, is the boundary of  $R^\ell$ .

(II) Given the offset regions  $R_k^\ell$  and  $R_{k+1}^\ell$  for  $k \in \mathbb{Z}^+$ ,

(a)  $R^\ell$  admits offset at distance  $k + \frac{1}{2}$  if any cell in  $R_{k+1}^\ell$  is related to  $R_k^\ell$  through one of the three connections shown in Figure 8; if this is the case, the offset curve at distance  $k + \frac{1}{2}$ , indicated as  $C_{k+\frac{1}{2}}$ , is the piecewise linear curve obtained by collecting together the contributions of any cell as shown in Figure 8;

(b)  $R^\ell$  admits offset at distance  $k + 1$  if the relationship between any cell in  $R_{k+1}^\ell$  and  $R_k^\ell$  falls into one of the three cases shown in Figure 9; if this is the case, the offset curve at distance  $k + 1$ , indicated as  $C_{k+1}$ , is the piecewise linear curve defined by the exterior boundary of  $R_{k+1}^\ell$ .

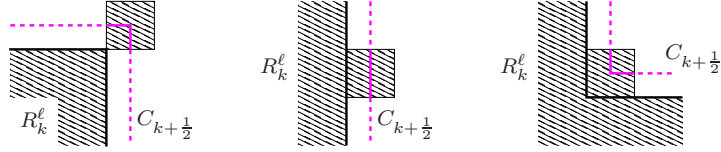


Figure 8: Admissible connections between a cell of  $R_{k+1}^\ell$  and the offset region  $R_k^\ell$  for defining the offset at distance  $k + \frac{1}{2}$ : one point (left), one side (center), and two adjacent sides (right). The piecewise linear contributions to the offset curve with respect to any of the three cases are also shown (magenta line).

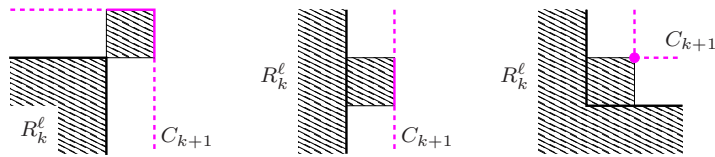


Figure 9: Admissible connections between a cell of  $R_{k+1}^\ell$  and the offset region  $R_k^\ell$  for defining the offset at distance  $k + 1$ : two free sides (left), one free side (center), and one free point (right), where free means that the edge or the vertex belongs to the boundary of  $\bigcup_{j=0}^{k+1} R_j^\ell$ . The piecewise linear contributions to the offset curve with respect to the three admissible cases are also shown (magenta line).

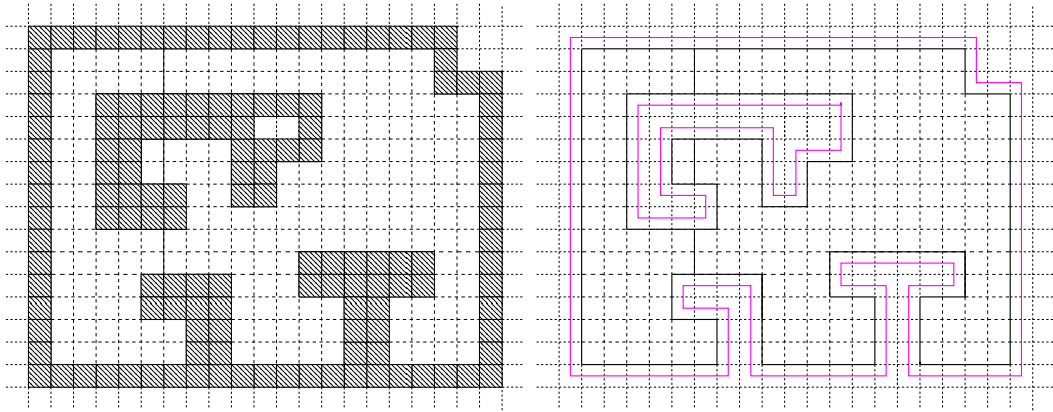


Figure 10: Offset region  $R_1^\ell$  (hatched cells on the left) to the ring  $R^\ell$  considered in Figure 6, and the corresponding offset curve  $C_{\frac{1}{2}}^\ell$  (magenta line on the right). According to Definition 15,  $R^\ell$  does not admit an offset at distance greater than  $\frac{1}{2}$ .

If one of the conditions (a) or (b) in the above Definition is not satisfied, then the ring  $R^\ell$  does not admit an offset at distance greater or equal to  $k + \frac{1}{2}$  or  $k + 1$ , respectively. These conditions allow to guarantee that the piecewise linear curve which defines the offset at a certain distance is *self-intersection free*. This property is needed to ensure that the basis counting we are going to introduce is always feasible. Figure 10 shows a simple example of offset region and offset curve to the ring considered in Figure 6.

**Definition 16.** *The length of an offset curve is the number of odd or even anchors that hit the offset itself.*

Let  $C_k^*$  be the offset at distance  $k$  to a connected component of the ring or to one of its holes. We define the *extremal* corners of  $C_k^*$  to be the following four corners:

- the highest  $\ulcorner$  and the lowest  $\llcorner$  of the leftmost corners of  $C_k^*$ ,
- the highest  $\urcorner$  and the lowest  $\lrcorner$  of the rightmost corners of  $C_k^*$ ,

The remaining part of  $C_k^*$  is characterized by a certain number of left corners ( $L_c$ ) and right corners ( $R_c$ ). At left/right corners, the length of  $C_{k+1}$  or  $C_{k+\frac{1}{2}}$  increases/decreases by 2 or 1, respectively. Using similar arguments as in the proof of Lemma 11, we may observe that the invariant property of a domain composed of  $M$  connected components,  $H$  holes,  $l$  left turns and  $r$  right turns, is that

$$l - r = 4M - 4H. \quad (11)$$

When  $C_k^*$  is the offset to a connected component of the boundary, assuming  $C_k^*$  to be counterclockwise oriented, the number of left corners always exceeds the number

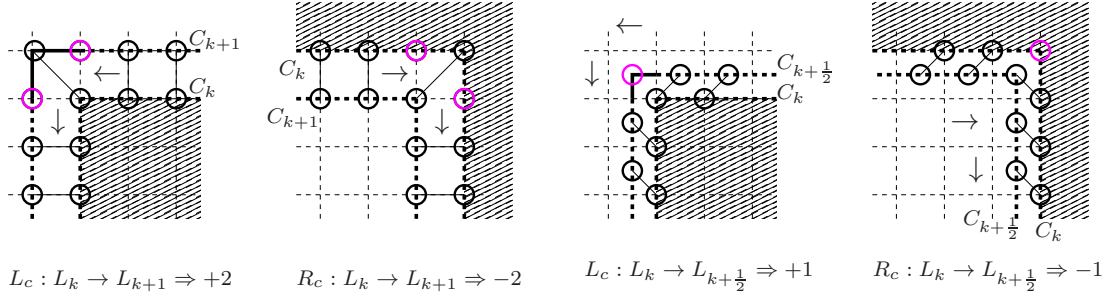


Figure 11: Classification of the corners along the offset curve and influence on the computation of the length according to Definition 16.

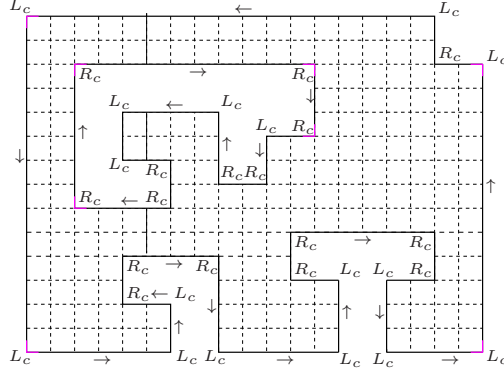


Figure 12: Corner classification for the ring shown in Figure 6: distinction between left ( $L_c$ ) and right ( $R_c$ ) corners. In this case:  $M = H = 1$ ,  $L_c = R_c = 16$ , and  $L_0 = L_{\frac{1}{2}} = 138$ .

of right corners by 4 (see Figure 12). When  $C_k^*$  is the offset to a hole, in order to keep the classification of the corners shown in Figure 11 valid, we assume  $C_k^*$  to be clockwise oriented. In this case, the number of right corners always exceeds the number of left corners by 4 (see again Figure 12). In both cases the number 4 is given by the extremal corners of the piecewise linear curve. This explains the terms  $+4M$  and  $-4H$  in equations (11).

**Lemma 17.** *The length of the offset curve to the ring can be recursively computed as follows.*

- (I) *Base case: the length of  $C_0$  is equal to the perimeter of the ring, i.e.,  $L_0 = p$ .*
- (II) *Recursive case: given the length of the offset curve at distance  $k \in \mathbb{Z}^+$ , indicated*

as  $L_k$ ,

$$L_{k+\frac{1}{2}} = L_k + 4M - 4H, \quad L_{k+1} = L_k + 8M - 8H. \quad (12)$$

*Proof.* In virtue of Figure 11, we have

$$L_{k+1} = L_k + 2(l - r), \quad L_{k+\frac{1}{2}} = L_k + l - r.$$

By substituting (11) into the above relations, we obtain the two recursive equations in (12).  $\square$

We may observe that

$$L_k = p + 8k(M - H), \quad L_{k+\frac{1}{2}} = p + 4(2k + 1)(M - H).$$

From the above relations we can compute the two sums

$$\sum_{k=0}^n L_k = (n + 1)p + 4n(n + 1)(M - H), \quad (13)$$

$$\sum_{k=0}^n L_{k+\frac{1}{2}} = (n + 1)p + 4(n + 1)^2(M - H), \quad (14)$$

which will be used in the proof of Theorem 19.

## 4.2 Enumerating the basis functions

According to the previous analysis, the second assumption on the domain configuration is as follows.

**Assumption 2.** *The ring  $R^\ell$  admits offsets at distance less or equal to  $(d - 1)/2$  with respect to the grid  $G^\ell$ .*

This means that even bi-degrees  $(d, d) = (2n, 2n)$  require offsets at distance  $n - \frac{1}{2}$ , while odd bi-degrees  $(d, d) = (2n + 1, 2n + 1)$  require offsets at distance  $n$ .

Let an *offset-segment* be the segment between two consecutive odd or even anchors along the offset curve at distance  $k$  or  $k + \frac{1}{2}$ , respectively, for any  $k = 0, 1, \dots$ . We may observe that the offsetting procedure preserves the number of MHCs. This means that for any MHC along the ring  $R^\ell$  there exists a corresponding MHC along each offset curve that  $R^\ell$  admits. Moreover, for any *lower* MHC along  $R^\ell$  with two boundary conditions and composed of  $n$  elementary horizontal segments, the corresponding MHC along the offset curve at distance  $(d - 1)/2$  consists of  $m = n - (d - 1)$  offset-segments.

**Remark 18.** *If the ring  $R^\ell$  satisfies Assumption 2, then it also satisfies Assumption 1.*

*Proof.* If the domain admits offsets at distance less or equal to  $(d - 1)/2$ , the number  $m$  of offset-segments along any MHC along the offset curve at distance  $(d - 1)/2$ , which corresponds to a lower MHC with two boundary conditions along the boundary of  $R^\ell$ , is at least 1. The number  $n = m + d - 1$  of elementary horizontal segments which form this lower MHC along  $R^\ell$  is then greater or equal to  $d$ .  $\square$

We can formalize the counting of basis functions whose support has some non-empty intersections with  $R^\ell$  as follows.

**Theorem 19.** *The number of basis functions in the set*

$$\{\tau : \tau \in T^\ell \wedge \text{supp } \tau \cap R^\ell \neq \emptyset\} \quad (15)$$

is equal to  $D^\ell$  (see Theorem 13) provided that Assumption 2 holds. In this case, the set (15) when restricted to  $R^\ell$  forms a basis of  $S^\ell$ , hence

$$S^\ell = V^\ell \Big|_{R^\ell}, \quad (16)$$

where  $V^\ell \Big|_{R^\ell}$  denotes the space obtained by restricting the functions in the tensor-product spline space  $V^\ell$  (see beginning of Section 2.1) to the ring  $R^\ell$ .

*Proof.* As shown in Figure 1 for the low bi-degree cases, if  $d$  is even, i.e.,  $d = 2n$ , we identify each basis function with the central elementary cell of its support. The total number of basis functions in  $T^\ell$  whose support intersects with  $\Omega^0 \setminus \Omega^{\ell+1}$  is given by

$$c + \sum_{k=0}^{n-1} L_{k+\frac{1}{2}} \quad (17)$$

The first term counts all the basis function centered in a cell inside the domain. The second term instead counts each cell centered along offset curves at distances

$$\frac{1}{2}, 1 + \frac{1}{2}, \dots, n - \frac{1}{2}.$$

The support of B-splines centered on the cells along these offset curves overlaps with the domain (see also Figure 13). By substituting (14) into (17), we obtain

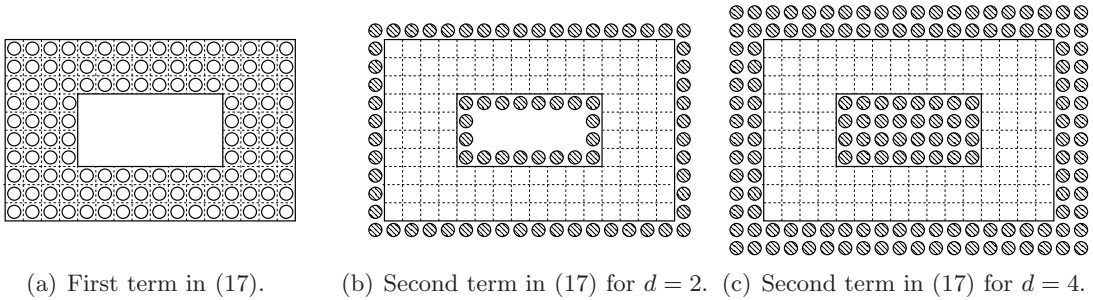
$$c + np + 4n^2(M - H) = c + \frac{d}{2}p + 4 \left(\frac{d}{2}\right)^2 (M - H) = D^\ell.$$

As already mentioned, when  $d$  is odd, i.e.,  $d = 2n + 1$ , we identify each basis function with the center of its support. The total number of basis functions in  $T^\ell$  which intersect with  $\Omega^0 \setminus \Omega^{\ell+1}$  is given by

$$\left(c - \frac{p}{2} + M - H\right) + \sum_{k=0}^n L_k \quad (18)$$

The first term counts all the basis function centered in a grid point inside the domain. The second term counts each cell centered along offset curves at distances

$$0, 1, \dots, n,$$



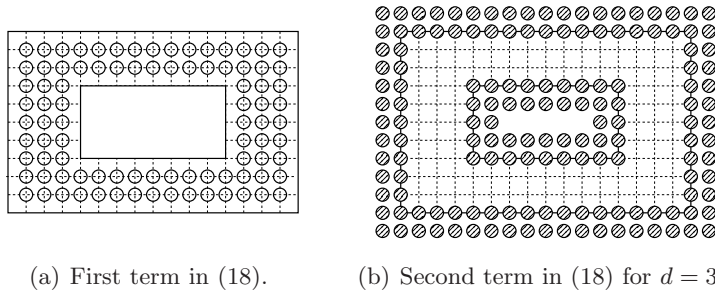
(a) First term in (17). (b) Second term in (17) for  $d = 2$ . (c) Second term in (17) for  $d = 4$ .

Figure 13: Number of tensor-product B-splines of bi-degree  $(2, 2)$  and  $(4, 4)$  whose supports intersect the domain.

i.e. that overlaps with the domain (see also Figure 14). By substituting (13) into (18), we obtain

$$c + \left(n + \frac{1}{2}\right)p + [4n(n + 1) + 1](M - H) = c + \frac{d}{2}p + 4\left(\frac{d}{2}\right)^2(M - H) = D^\ell.$$

Obviously, the functions in (15) are linearly independent, hence they form a basis of the space  $S^\ell$ .  $\square$



(a) First term in (18). (b) Second term in (18) for  $d = 3$ .

Figure 14: Number of tensor-product B-splines of bi-degree  $(3, 3)$  whose supports intersect the domain.

Figure 15 shows some admissible and non-admissible domain configurations.

## 5 Hierarchical bases on multi-grid multi-cell domains

The results obtained so far are valid only for the individual rings  $R^\ell$ , where all cells belong to the grid of the same spline space  $V^\ell$ . Now we turn our attention to the full multi-grid case. More precisely, we consider the space  $W$  of all spline functions of bi-degree  $(d, d)$  and maximal order of smoothness which exist on the multi-grid multi-cell

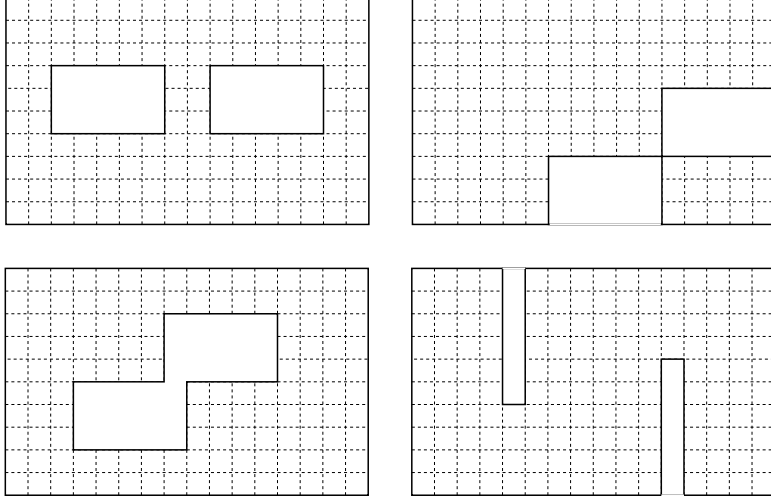


Figure 15: Examples of admissible (top) and non-admissible (bottom) domain configurations for  $d = 2$ .

domain obtained by restricting the grid of  $V^\ell$  to  $\Omega^\ell$ , see (4). We formulate the main result of this paper:

**Theorem 20.** *If Assumption 2 on the domain configuration holds for all rings  $R^\ell$  ( $\ell = 0, \dots, N - 1$ ) then the hierarchical B-spline basis  $\mathcal{K}$  introduced in Definition 1 spans the entire space  $W$  defined in Eq. (4).*

*Proof.* Given a function  $f \in W$ , we show that  $f \in \text{span} \mathcal{K} \Big|_{\Omega^0}$ . We proceed in three steps.

- Step 1: There exist  $N$  functions

$$f^\ell \in \text{span}\{\tau \in T^\ell : \text{supp } \tau \cap R^\ell \neq \emptyset\} \subseteq V^\ell, \quad \ell = 0, \dots, N - 1 \quad (19)$$

such that

$$f^\ell \Big|_{R^\ell} = \left( f - \sum_{i=0}^{\ell-1} f^i \right) \Big|_{R^\ell}. \quad (20)$$

This can be seen by induction over  $\ell$ . The existence of  $f^0$  is guaranteed by Theorem 19, as Assumption 2 holds for  $R^0$  and  $f \Big|_{R^0} \in S^0 = V^0 \Big|_{R^0}$ . Now, assuming that the existence of  $f^0, \dots, f^{\ell-1}$  was already shown, the same theorem also guarantees the existence of  $f^\ell$ . Indeed, Assumption 2 holds for  $R^\ell$ ,  $f \Big|_{R^\ell} \in W \Big|_{R^\ell} \subseteq S^\ell$ , and

$$f^i \Big|_{R^\ell} \in V^i \Big|_{R^\ell} \subseteq V^\ell \Big|_{R^\ell} = S^\ell, \quad i = 0, \dots, \ell - 1. \quad (21)$$

- Step 2: These functions satisfy

$$f^\ell \Big|_{R^{\ell-1}} = 0, \quad \ell = 0, \dots, N - 1, \quad (22)$$

where we set  $R^{-1} = \emptyset$  to include the case  $\ell = 0$ . Indeed, (20) can be rewritten as

$$f|_{R^\ell} = \sum_{i=0}^{\ell} f^i|_{R^\ell}, \quad (23)$$

and  $R^{\ell-1} \subseteq R^\ell$  then implies

$$f|_{R^{\ell-1}} = \sum_{i=0}^{\ell} f^i|_{R^{\ell-1}}. \quad (24)$$

Moreover, rewriting (20) for  $f^{\ell-1}$  yields

$$f|_{R^{\ell-1}} = \sum_{i=0}^{\ell-1} f^i|_{R^{\ell-1}}. \quad (25)$$

The claimed result (22) follows immediately when comparing equations (24) and (25).

• **Step 3:** These functions satisfy

$$f^\ell \in \text{span } \mathcal{K}^\ell = \text{span}\{\tau \in T^\ell : \text{supp } \tau \cap R^{\ell-1} = \emptyset \wedge \text{supp } \tau \cap R^\ell \neq \emptyset\}, \quad (26)$$

see (2). In order to prove this fact we consider a representation of  $f^\ell$  with respect to the basis considered in (19), namely

$$f^\ell = \sum_{\tau \in T^\ell, \text{supp } \tau \cap R^\ell \neq \emptyset} c_\tau \tau. \quad (27)$$

For any basis function  $\tau$  that has a non-empty intersection with  $R^{\ell-1}$ , the previous observation (22) implies that the corresponding coefficient  $c_\tau$  in (19) is necessarily zero, since the basis functions in  $T^\ell$  are locally linearly independent. This proves (26).

The proof of the theorem is complete, since  $\mathcal{K} = \bigcup_{\ell=0}^{N-1} \mathcal{K}^\ell$  and rewriting (20) for  $\ell = N-1$  gives

$$f|_{R^{N-1}} = \sum_{i=0}^{N-1} f^i|_{R^{N-1}}, \quad (28)$$

where  $R^{N-1} = \Omega^0$  and  $f^i \in \text{span } \mathcal{K}^i$ . □

**Remark 21.** 1. Note that the assumptions regarding the offsets are independent and refer to different grids. More precisely, the condition that  $R^\ell = \Omega^0 \setminus \Omega^{\ell+1}$  needs to admit certain offsets with respect to the grid  $G^\ell$  constrains only the selection of  $\Omega^{\ell+1}$  but does not impose conditions on any other subdomain  $\Omega^k$ ,  $k \neq \ell+1$ .

2. The hierarchical grids satisfying Assumption 2 make local refinement possible. To derive a simple construction, we assume that, for any level  $\ell$ , the number of cells in each direction is a multiple of  $d$ . We denote by **d-grid** of level  $\ell$  the aligned disjoint boxes composed of  $d \times d$  cells with respect to the grid of  $V^\ell$ . If  $\Omega^{\ell+1}$ , for  $\ell = 0, \dots, N-2$ , can be decomposed into a  $d$ -grid of level  $\ell$ , then Assumption 2 is satisfied. As shown in Figure 16 for  $d = 2$ , the class of hierarchical meshes with this property admits the possibility of a local refinement.

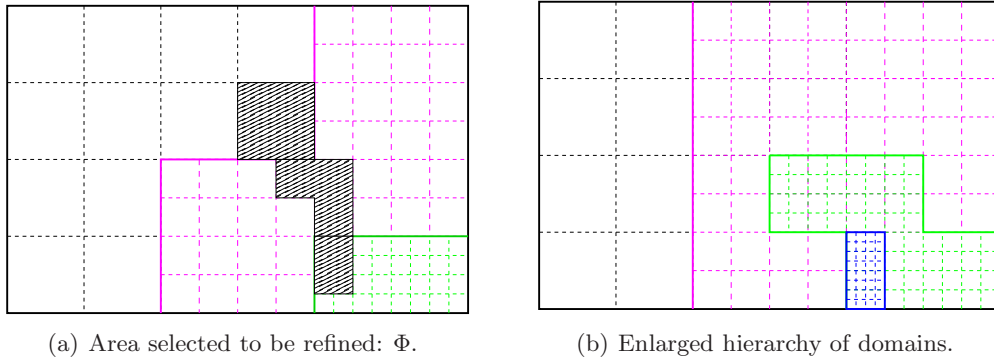


Figure 16: Left: a nested hierarchy of domains ( $N = 3$ ) where each sub-domain  $\Omega^{\ell+1}$  can be decomposed into a 2-grid of level  $\ell$ , and a region marked for refinement (hatched). Right: the enlarged nested hierarchy of domains ( $N = 4$ ).

## 6 Closure

The dimension of smooth bivariate hierarchical tensor-product B-spline spaces defined on multi-grid multi-cell domains given by sets of cells of tensor-product grids at different refinement levels has been studied. Theorem 20 states that bivariate hierarchical B-splines span the space of piecewise polynomials with the maximum order of smoothness defined on certain hierarchical grids.

A detailed analysis of the admissible domain configurations covered by the proposed analysis has been presented, leading to the formulation of Assumption 2. A simple approach to satisfy this assumption has been proposed, see Remark 21. The development of a more sophisticated algorithm based on weaker assumptions on the cell configuration may be the subject of further studies.

The hierarchical basis can be suitably modified in order to define a piecewise polynomial basis which is non-negative and consists of locally supported basis functions which also form a partition of unity. The possibility of modifying the basis functions to define a normalized *weighted* basis is discussed in [24].

## Acknowledgments

The research leading to these results has received funding from the European Union Seventh Framework Programme (FP7/2007-2013) under grant agreements n°214584 (SAGA) and n°272089 (PARADISE).

## References

- [1] Y. Bazilevs, V. M. Calo, J. A. Cottrell, J. Evans, T. J. R. Hughes, S. Lipton, M. A. Scott, and T. W. Sederberg. Isogeometric analysis using T-splines. *Computer*

- Methods in Applied Mechanics and Engineering*, 199:229–263, 2010.
- [2] A. Buffa, D. Cho, and G. Sangalli. Linear independence of the T-spline blending functions associated with some particular T-meshes. *Computer Methods in Applied Mechanics and Engineering*, 199:1437–1445, 2010.
  - [3] J. A. Cottrell, T. J. R. Hughes, and Y. Bazilevs. *Isogeometric Analysis: Toward Integration of CAD and FEA*. John Wiley & Sons, 2009.
  - [4] J. Deng, F. Chen, and Y. Feng. Dimensions of spline spaces over T-meshes. *Journal of Computational and Applied Mathematics*, 194:267–283, 2006.
  - [5] J. Deng, F. Chen, X. Li, Ch. Hu, W. Tong, Z. Yang, and Y. Feng. Polynomial splines over hierarchical T-meshes. *Graphical Models*, 70:76–86, 2008.
  - [6] M. R. Dörfel, B. Jüttler, and B. Simeon. Adaptive isogeometric analysis by local h-refinement with T-splines. *Computer Methods in Applied Mechanics and Engineering*, 199:264–275, 2010.
  - [7] D. R. Forsey and R. H. Bartels. Hierarchical B-spline refinement. *Computer Graphics*, 22:205–212, 1988.
  - [8] D. R. Forsey and R. H. Bartels. Surface fitting with hierarchical splines. *ACM Transactions on Graphics*, 14:134–161, 1995.
  - [9] D. R. Forsey and D. Wong. Multiresolution surface reconstruction for hierarchical B-splines. In Wayne A. Davis, Kellogg S. Booth, and Alain Fournier, editors, *Graphics Interface*, pages 57–64. Canadian Human-Computer Communications Society, 1998.
  - [10] G. Greiner and K. Hormann. Interpolating and approximating scattered 3D-data with hierarchical tensor product B-splines. In A. Le Méhauté, C. Rabut, and L. L. Schumaker, editors, *Surface Fitting and Multiresolution Methods*, Innovations in Applied Mathematics, pages 163–172. Vanderbilt University Press, Nashville, TN, 1997.
  - [11] T. J. R. Hughes, J. A. Cottrell, and Y. Bazilevs. Isogeometric analysis: CAD, finite elements, NURBS, exact geometry and mesh refinement. *Computer Methods in Applied Mechanics and Engineering*, 194:4135–4195, 2005.
  - [12] R. Kraft. Adaptive and linearly independent multilevel B-splines. In A. Le Méhauté, C. Rabut, and L. L. Schumaker, editors, *Surface Fitting and Multiresolution Methods*, pages 209–218. Vanderbilt University Press, Nashville, 1997.
  - [13] R. Kraft. *Adaptive und linear unabhängige Multilevel B-Splines und ihre Anwendungen*. PhD thesis, Universität Stuttgart, 1998.

- [14] X. Li, J. Deng, and F. Chen. Polynomial splines over general T-meshes. *Visual Computer*, 26:277–286, 2010.
- [15] X. Li and M. A. Scott. On the nesting behavior of T-splines. Technical Report 11-13, ICES, 2011.
- [16] X. Li, J. Zheng, T. W. Sederberg, T. J. R. Hughes, and M. A. Scott. On linear independence of T-spline blending functions. *Computer Aided Geometric Design*, 29:63–76, 2012.
- [17] B. Mourrain. On the dimension of spline spaces on planar T-subdivisions. 2010. URL <http://hal.inria.fr/inria-00533187/en>.
- [18] N. Nguyen-Thanh, H. Nguyen-Xuan, S. P. A. Bordas, and T. Rabczuk. Isogeometric analysis using polynomial splines over hierarchical T-meshes for two-dimensional elastic solids. *Computer Methods in Applied Mechanics and Engineering*, 200:1892–1908, 2011.
- [19] L. Schumaker. *Spline functions: basic theory*. Cambridge University Press, 2007.
- [20] M. A. Scott, M. J. Borden, C. V. Verhoosel, T. W. Sederberg, and T. J. R. Hughes. Isogeometric finite element data structures based on Bézier extraction of T-splines. *International Journal for Numerical Methods in Engineering*, 88:126–156, 2011.
- [21] M. A. Scott, X. Li, T. W. Sederberg, and T. J. R. Hughes. Local refinement of analysis-suitable T-splines. *Computer Methods in Applied Mechanics and Engineering*, 213–216:206–222, 2012.
- [22] T. W. Sederberg, D. L. Cardon, G. T. Finnigan, N. S. North, J. Zheng, and T. Lyche. T-spline simplification and local refinement. *ACM Transactions on Graphics*, 23:276 – 283, 2004.
- [23] T. W. Sederberg, J. Zheng, A. Bakenov, and A. Nasri. T-splines and T-NURCCS. *ACM Transactions on Graphics*, 22:477–484, 2003.
- [24] A.-V. Vuong, C. Giannelli, B. Jüttler, and B. Simeon. A hierarchical approach to adaptive local refinement in isogeometric analysis. *Computer Methods in Applied Mechanics and Engineering*, 200:3554–3567, 2011.